ISSN 1070-3284, Russian Journal of Coordination Chemistry, 2019, Vol. 45, No. 1, pp. 74–79. © Pleiades Publishing, Ltd., 2019.

An Uncommon Nanocage 3D Metal–Organic Framework Built from a Tetracarboxylate Ligand: Photoluminescence and Photocatalytic Properties[1]

J. Feng[a], S. R. Fan[b], Z. Z. Li[a], S. Z. Yang[b], W. K. Luo[b], and X. R. Wu[b, *]

[a] *Department of Mechanical and Electrical Engineering, Guangdong University of Science & Technology, Dongguan, 523083 P.R. China*

[b] *Dongguan Key Laboratory of Drug Design and Formulation Technology, Key Laboratory of Research and Development of New Medical Materials of Guangdong Medical University, School of Pharmacy, Guangdong Medical University, Dongguan, 523808 P.R. China*

**e-mail: wuxiren2000@163.com*

Received March 2, 2018; revised April 7, 2018; accepted April 19, 2018

Abstract—A new Eu(II)-based complex $[H_2N(Me)_2][Eu_3(L)_2(HCOO)_2(DMF)_2(H_2O)]$(I) ($H_4L$ = 3,5'-di(3',5'-dicarboxylphenyl)pyridine) has been synthesized and structurally characterized. Single-crystal X-ray analysis (CIF file CCDC no. 1559225) reveals that compound **I** has 3D $(4.6^2)(4.6^2)(4^2.6^7.8^6)$ topology. The emission spectra of **I** is dominated by four characteristic bands and shows strong luminescent feature. Furthermore, the photocatalytic properties of **I** for degradation of the methyl violet and Rhodamine B have been explored.

Keywords: structure, photocatalytic properties, luminescence

DOI: 10.1134/S1070328419010019

INTRODUCTION

The rapidly expanding field of crystal engineering of multidimensional metal-organic frameworks (MOFs) is of great current interest for their specific structural features and potential applications [1, 2]. Recently, MOFs could show great potential for semiconductor photocatalysis (e.g. dye degradation), which is recognized as one of the most promising solutions to address the world-wide environmental [3]. Alvaro et al. studied the photocatalytic properties of MOF-5 in the degradation of phenol in aqueous solutionin 2007 [4], Latterly, Laruri et al. first reported the iron(III)-based MOFs can photodegrade Rhodamine 6G in aqueous solution under visible light irradiation [5]. However, despite it still being significant challenge, there is an urgent need to design and tailor MOFs with practical applications rationally and delicately [6].

Conformationally non-rigid *exo*-bidentate ligand, such as 5-nitro-1,3-benzenedicarboxylic acid is a rigid planar molecule containing two *exo*-carboxylicacid groups, forming a 120° molecular component and has been extensively used in the synthesis of multidimensional MOFs containing a large variety of metal centers [7–9]. To further understand the coordination chemistry of the rigid aromatic carboxylate acid, to evaluate the influence of different coordination geometryof metal ions on the resulting framework and to explore new materials with beautiful architectures and good physical properties. In this work, 3,5'-di(3',5'-dicarboxylphenyl)pyridine (H_4L) has been introduced to the trivalent metal ions Eu^{3+} system. As a result, a new 3D coordination polymer has been obtained under hydrothermal conditions, namely, $[H_2N(Me)_2][Eu_3(L)_2(HCOO)_2(DMF)_2(H_2O)]$ (**I**). The crystal structure and topological analyses of **I** has been represented and discussed. In addition, the fluorescent and photocatalytic properties of **I** have also been investigated below in detail.

EXPERIMENTAL

Materials and methods. All chemicals were purchased from Jinan Henghua Sci. and Tec. Co. Ltd. without further purification. IR spectra were recorded with a Perkin-Elmer Spectrum One spectrometer in the region 4000–400 cm^{-1} using KBr pellets. Thermogravimetric (TG) analysis was carried out with a Metter-Toledo TA 50 under dry dinitrogen flux (60 mL min^{-1}) at a heating rate of 5°C min^{-1}. X-ray powder diffraction (XRPD) data were recorded on a Rigaku RU200 diffractometer at 60 kV, 300 mA for CuK_α radi-

[1] The article is published in the original.

Table 1. Crystallographic data and structure refinement for complex **I**

Parameter	Value
Formula weight	480.20
Crystal system	Cubic
Space group	$Im\overline{3}$
Unit cell dimensions:	
a, Å	38.1260(13)
b, Å	38.1260(13)
c, Å	38.1260(13)
Volume, Å^3; Z	55420(6); 26
ρ(calcd.), mg/cm^3	1.094
F(000)	17805
θ Range for data collection, deg	2.10–25.18
Limiting indices	$-49 \le h \le 49$, $-41 \le k \le 49$, $-49 \le l \le 49$
Reflections collected	252910
Independent reflections (R_{int})	11102 (0.0984)
Reflections with $I > 2\sigma(I)$	9386
Numder of refinement	1485
Completeness, %	97.5
Goodness-of-fit on F^2	1.097
Final R indices ($I > 2\sigma(I)$)	$R_1 = 0.0773$, $wR_2 = 0.2159$
R indices, all data	$R_1 = 0.0984$, $wR_2 = 0.2393$
$\Delta\rho_{max}/\Delta\rho_{min}$, e Å^{-3}	3.522/–2.121

ation (λ = 1.5406 Å) witha scan speed of 2°C/min and a step size of 0.02° in 2θ.

Synthesis of I. A mixture of H_4L (16.82 mg) and $Eu(NO_3)_3 \cdot 6H_2O$ (185.60 mg) was dissolved in DMF (3 mL) in a screw-capped vial. After two drops of HNO_3 (63%, aq.) were added to the mixture, the vial was capped and placed in an oven at 105°C for 12 h. Theresulting single crystals were washed with DMF three times to give **I**. The yield was ~35 mg (based on H_4L). IR (KBr; ν, cm^{-1}): 3134 s, 2900 m, 2452 w, 2367 w, 2096 w, 1658 m, 1552 m, 1448 w, 1392 s, 1279 m, 1099 s, 1062 m, 933 m, 860 m,788 s, 729 s, 663 s, 518 m.

X-ray crystallography. X-ray diffraction measurements were carried out on a Bruker SMART APEX diffractometer that was equipped with a graphitemonochromated MoK_α radiation (λ = 0.71073 Å) by using an ω-scan technique. The intensities were corrected absorption effects by using SADABS. The structures were solved by using SHELXS-97 and refined by using SHELX-97 [10]. Absorption correction sapplied by using multi-non-hydrogen atoms were refined anisotropically. For **I**, the unit cell exhibits large regions that are occupied by solvent molecules; the solvent molecules could not be modeled.

The SQUEEZE option in PLATON [11] was used toproduce a set of solvent-free diffraction intensities.The nature and number of solvent molecules wereestablished from C, H, and N elemental analyses and TG analyses. Crystallographic details aregiven in Table 1. Selected bond dimensions are listed in Table 2.

Supplementary material for structure **I** has been deposited with the Cambridge Crystallographic Data Centre (CCDC no. 1559225; deposit@ccdc.cam.ac.uk or http://www.ccdc.cam.ac.uk).

RESULTS AND DISCUSSION

The asymmetric unit of **I** has two independent Eu^{3+} ions, two L ligands, two formate anions, one DMF and one aqua molecule (Fig. 1). Eu(1) is nine-coordinated by one aqua ligand and eight O atoms of two formate groups and four carboxylate groups from four L ligands, displaying a monocapped square antiprism geometry. Eu(2) shows a bicapped trigonal prism geometry defined by six O atoms of four carboxylate groups from four L ligands, one O atom of the formate group, and one DMF ligand. The structure of **I** contains Eu_3 clusters in which the metal atoms are connected by carboxylate groups from L ligands and a μ_4

Table 2. Selected bond lengths (Å) and angles (deg) for complex **I***

Bond	*d*, Å	Bond	*d*, Å
Eu(1)–O(11*A*)	2.329(12)	Eu(1)–O(9*A*)	2.357(11)
Eu(1)–O(13)	2.44(3)	Eu(1)–O(7*A*)	2.66(3)
Eu(1)–O(8)	2.47(2)	Eu(1)–O(5)	2.565(7)
Eu(1)–O(6*A*)	2.59(3)	Eu(2)–O(12*A*)	2.35(2)
Eu(2)–O(10*B*)	2.35(3)	Eu(2)–O(2)	2.364(12)
Eu(2)–O(2)	2.372(18)	Eu(2)–O(5)	2.385(6)
Eu(2)–O(1*B*)	2.386(16)	Eu(2)–O(14)	2.436(6)
Eu(2)–O(4)	2.474(12)		
Angle	ω, deg	Angle	ω, deg
O(11*A*)Eu(1)O(8)	138.0(4)	O(5)Eu(1)O(6*A*)	148.1(4)
O(11)Eu(1)O(6)	110.0(6)	O(11)Eu(1)O(9*A*)	74.7(4)
O(9*B*)Eu(2)O(5)	124.1(4)	O(12*B*)Eu(2)O(2)	148.7(6)
O(12*A*)Eu(2)O(3)	88.9(10)	O(3)Eu(2)O(5)	127.8(4)
O(1*B*)Eu(2)O(5)	124.9(4)	O(5)Eu(2)O(14)	141.8(2)

* Symmetry transformations used to generate equivalent atoms: (*A*) *x*, *y*, *z*; (*B*) *x*, –*y*, –*z*.

formate anion (Fig. 2a). The L ligands in turn coordinate to three Sm_3 clusters, two via a single carboxylate group each, and one through two carboxylate groups. The ligands thus acts as a 3-connecting nodes, while the Eu_3 cluster is coordinated by eight carboxylates from six L ligands. This generates a 3D network with two different 3-connecting ligand nodesand 6-connecting Eu_3 nodes (Fig. 2b). It has $(4.6^2)(4.6^2)(4^2.6^7.8^6)$ topology. The most interesting feature is that twelve Eu_3 clusters and twelve L linkers interlink to form a nanocage (cage A), while twelve Eu_3 clusters, eight N(2) pyridine-containing and four N(1) pyridine-containing L linkers interconnect to form another nanocage (cage B). The cages A and B arrange along the cubic cell axes; as a result, another octahedral nanocage (cage **C**) with a diameter of 1.1 nm is formed among them by six Eu_3 clusters and twelve isophthalate units of twelve L linkers (Fig. 2b). This structure is very similar with the recent work [12, 13].

As to FT-IR spectra, **I** shows abroad band centered around 3200 cm^{-1} attributable to the O–H stretching frequency of the water molecule. Specifically, asymmetric stretching vibration $\nu(COO^-)$ appear around 1680 cm^{-1}, and the symmetric stretching vibration $\nu(COO^-)$ are observed at 1552 cm^{-1}. The difference between the asymmetric and symmetric stretches, $\Delta = \nu_{as}(COO^-) - \nu_s(COO^-)$, are on the order of 120 cm^{-1} indicating that carboxyl groups are coordinated to the metal in a bidentate modes [14], consistent with the observed X-ray crystal structures of **I**.

To study the stability of the polymers, TG analysisof **I** was performed. The TGA result of **I** shows two weight loss steps. A total weight lossof 24.3% at 32–269°C, corresponding to the loss of 2.5DMF and $19H_2O$ guest molecules performula unit (calcd. 24.7%). Above 320–390°C, these frameworks begin tocollapse with the loss of other organic molecules.

The solid-state emission spectra of **I** at room temperature are shown in Fig. 3. When excited at 310 nm, **I** exhibits four characteristic transitions of Eu^{3+} ion: 593, 614, 697, and 705 nm, ascribed to$^5D_0 \rightarrow {}^7F_J$ (J = 1–4) [15–17], respectively. The strongest $^5D_0 \rightarrow {}^7F_2$ transition is an electric dipole transition, the so-called hypersensitive transition, and is responsible for the brilliant redemission. Although the magnetic dipole transition of $^5D_0 \rightarrow {}^7F_1$, which is fairly insensitive to the coordination environment of the Eu^{3+} ion, is also present, it is clearly less intense than the $^5D_0 \rightarrow {}^7F_2$ transition. The above results suggest the absence of inversion symmetry of Eu^{3+} sites in **I**, which is in agreement with the single-crystal X-ray analysis.

These methyl violet (MV) and Rhodamine B (RhB) were selected as model organic contaminant to study the photocatalytic activities of **I**. As shown in Fig. 4, the absorption peaks of MV and RhB decrease obviously with the increasing of reaction time in the presence of **I**. The calculation results show that the degradation rate of MV is 77.8%, while for RhB, the degradation rate is 55.3%. In addition, the control experiments on the degradation of organic pollutants were examined in the same reaction condition just without catalyst. The degradation rate of MV and RhB is just 18.3 and 21.6% within 100 min under UV irradiation without catalyst. As the above photocatalytic results shown, the photocatalytic performance of **I** for MV is the better than those of RhB. After photocatalysis, the PXRD patterns of **I** are similar with the sim-

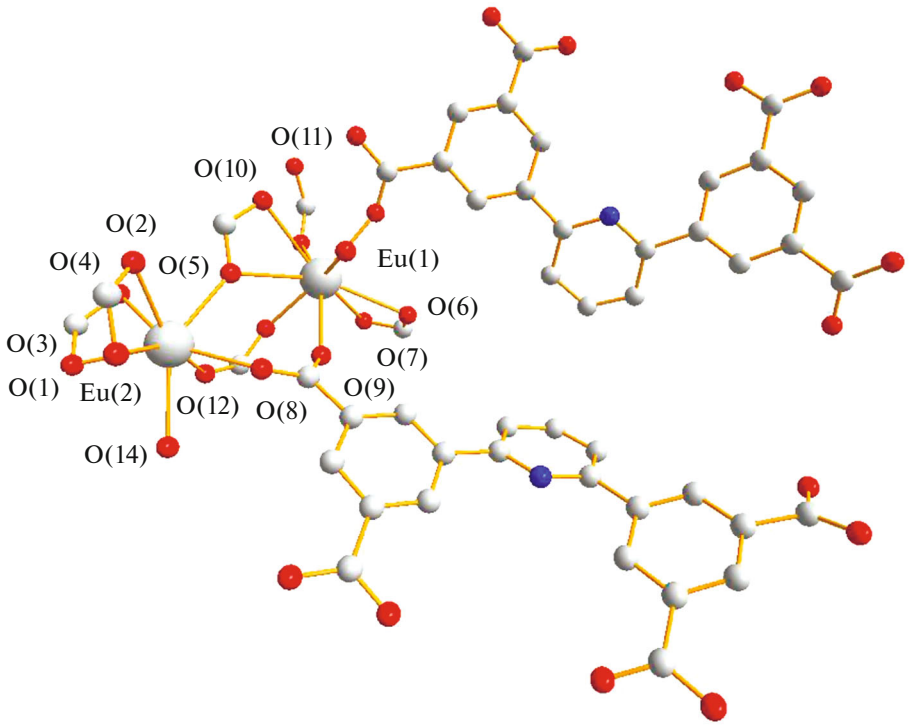

Fig. 1. Coordination environments of Eu^{3+} ions.

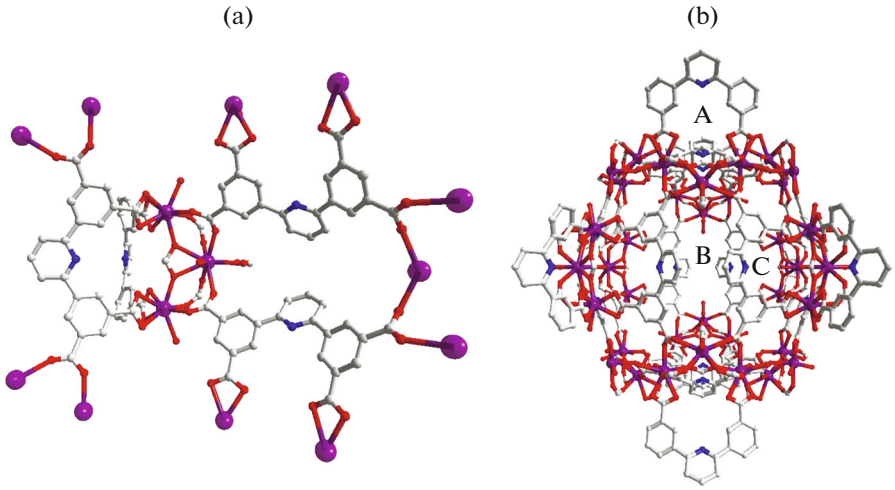

Fig. 2. Local ligand and metal coordination geometries in the structure (a) and interlinked 3D pore with A, B, C nanocages (b).

ulated one, implying that **I** maintains its structural interlinkage after the photocatalysis reaction. The possible photocatalytic mechanism is that when absorbed energy equal to or higher than its band gap energy (LUMO and the HOMO) of the materials **I**. When the HOMO seized one electron from one water molecule and then go back to stable state. The water molecule was oxidized into a ·OH. Meanwhile, the electron of the LUMO reduced one O_2 to one O_2^- by the combination of electrons (e−), which also turned to ·OH. Finally, full ·OH radical active works as an oxidizing agent to decompose MV/RhB [18–22].

In summary, we have successfully synthesized a 3D nanocage MOF. High stability and recyclability of **I** make their outstanding candidates in the field of photocatalytic activities. The present work opens a promising approach to design photocatalytic reaction; this will probably be useful under more realistic conditions in the future.

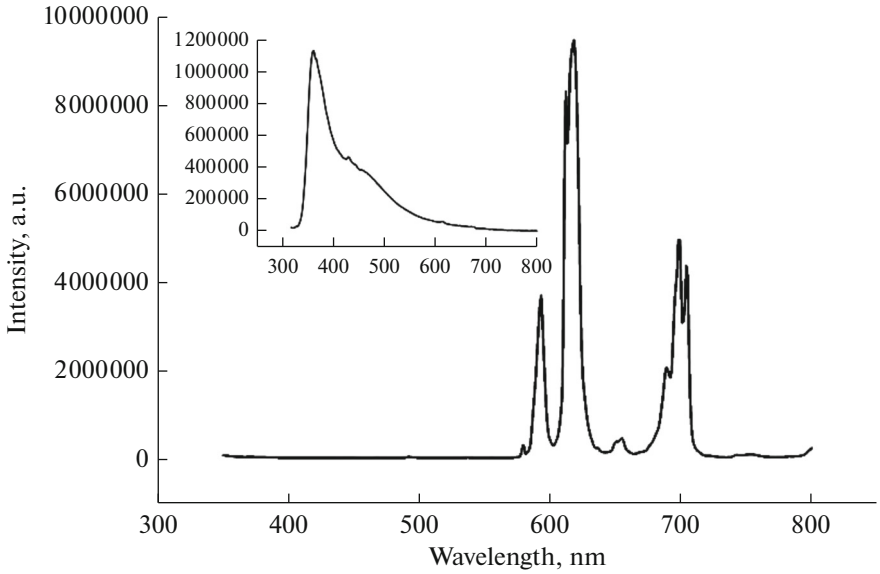

Fig. 3. Solid state emission spectra of **I** at room temperature.

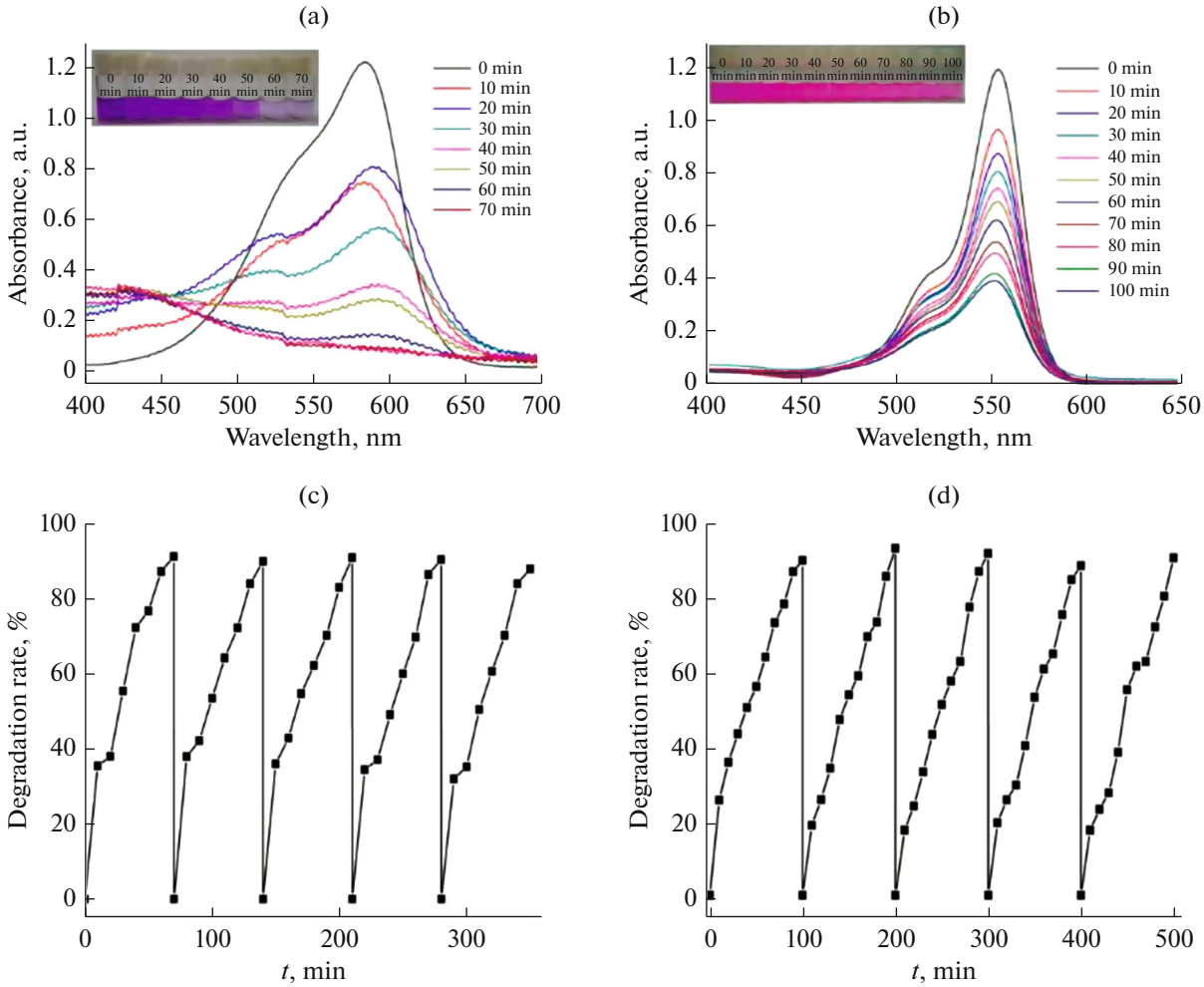

Fig. 4. UV-Vis absorption spectra of the MV (a) and RhB (b) solution during the decomposition reaction under 500 W Hg lamp irradiation in the presence of **I**; the recycle experimental work for MV: (c) and(d), respectively.

ACKNOWLEDGMENTS

This work was partially supported by the grants from NSF of China (no. 21701033), Science Foundation funded project of Guangdong Medical University (Z2016001 and M2016023), Innovative Entrepreneurial Training Plan of undergraduates in Guangdong Province (nos. 201710571005, 201710571007; 201710571012; 201710571016; 201710571008; 201710571020, 201710571060) and Innovation experiment project of Guangdong Medical University (ZYDM024), Special Funds for Scientificand Technological Innovation of undergraduates in Guangdong Province (pdjha0218, pdjha0219, pdjha0226), and Innovative talent project of Guangdong provincial universities (2015KQNCX189).

REFERENCES

1. Guo, J., Yang, J., Liu, Y.Y., and Ma, J.F., *CrystEngComm*, 2012, vol. 14, p. 6609.
2. Tu, J.P., Zeng, X.L., Xu, F.J., et al., *Chem. Commun.*, 2017, vol. 53, p. 3361.
3. Sun, W., Wang, J.Z., Zhang, G.N., and Liu, Z.L., *RSC Adv.*, 2014, vol. 4, p. 55252.
4. Alvaro, M., Carbonell, E., Ferrer, B., et al., *Chem. Eur. J.*, 2007, vol. 13, p. 5106.
5. Laurier, K.G.M., Vermoortele, F., Ameloot, R., et al., *J. Am. Chem. Soc.*, 2013, vol. 135, p. 14488.
6. Dias, E.M. and Petit, C., *J. Mater. Chem., A*, 2015, vol. 3, p. 22484.
7. Wang, D.E., Deng, K.J., Lv, K.L., et al., *CrystEngComm*, 2009, vol. 11, p. 1442.
8. Abourahma, H., Moulton, B., Kravtsov, V., and Zaworotko, M.J., *J. Am. Chem. Soc.*, 2002, vol. 124, p. 9990.
9. Ye, J.W., Wang, J., Zhang, J.Y., et al., *CrystEngComm*, 2007, vol. 9, p. 515.
10. Sheldrick, G.M., *Acta Crystallogr., Sect. A: Found. Crystallogr.*, 2008, vol. 64, p. 112.
11. Spek, A.L., *J. Appl. Crystallogr.*, 2015, vol. 71, p. 9.
12. Liu, B., Wu, W.P., Hou, L., and Wang, Y.Y., *Chem. Commun.*, 2014, vol. 50, p. 8731.
13. Liu, J.Q., Li, X.F., Gu, C.Y., et al., *Dalton Trans.*, 2015, vol. 44, p. 19370.
14. Yu, X.F., Lu, L., Zhong, Y.R., et al., *Russ. J. Coord. Chem.*, 2017, vol. 43, p. 244. doi 10.1134/S1070328417040091
15. Tian, F.Y., Liu, G.H., Li, B., et al., *Russ. J. Coord. Chem.*, 2017, vol. 43, p. 304. doi 10.1134/S1070328417050074
16. Zhou, M.J., Shi, W., Xu, N., and Cheng, P., *Inorg. Chem.*, 2013, vol. 52, p. 8082.
17. Vicentini, G., Zinner, L.B., Zukerman-Schpector, J., and Zinner, K., *Coord. Chem. Rev.*, 2000, vol. 196, p. 353.
18. Jin, J.C., Wu, J., Liu, W.C., et al., *New J. Chem.*, 2018, vol. 42, p. 2767.
19. Wu, J., Li, B.H., Zhong, H.R., et al., *J. Mol. Struct.*, 2018, vol. 1158, p. 264.
20. Wu, Y., Wu, J., Luo, Z.D., et al., *RSC Advances*, 2017, vol. 7, p. 10415.
21. Wu, W.P., Wu, J., Liu, J.Q., et al., *RSC Advances*, 2017, vol. 7, p. 54522.
22. Wang, X.L., Luan, L., Lin, H.Y., et al., *Dalton Trans.*, 2013, vol. 42, p. 8375.